# Reuse of Red Algae Waste for the Production of Cellulose Nanocrystals and its Application in Polymer Nanocomposites

Mounir El Achaby, Zineb Kassab, Adil Aboulkas, Cedric Gaillard, Abdellatif Barakat

# Accepted Manuscript

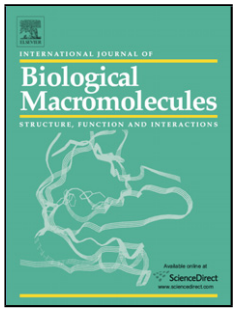


Title: Reuse of Red Algae Waste for the Production of Cellulose Nanocrystals and its Application in Polymer Nanocomposites

Authors: Mounir El Achaby, Zineb Kassab, Adil Aboulkas, Cédric Gaillard, Abdellatif Barakat

PII: S0141-8130(17)32490-X
DOI: http://dx.doi.org/doi:10.1016/j.ijbiomac.2017.08.067
Reference: BIOMAC 8059

To appear in: *International Journal of Biological Macromolecules*

Received date: 9-7-2017
Revised date: 9-8-2017
Accepted date: 10-8-2017

Please cite this article as: Mounir El Achaby, Zineb Kassab, Adil Aboulkas, Cédric Gaillard, Abdellatif Barakat, Reuse of Red Algae Waste for the Production of Cellulose Nanocrystals and its Application in Polymer Nanocomposites, International Journal of Biological Macromoleculeshttp://dx.doi.org/10.1016/j.ijbiomac.2017.08.067

# Reuse of Red Algae Waste for the Production of Cellulose Nanocrystals and its Application in Polymer Nanocomposites

Mounir El Achaby[1,*], Zineb Kassab[1], Adil Aboulkas[1,2], Cédric Gaillard[3], Abdellatif Barakat[1,4]

[1]Materials Science and Nanoengineering (MSN) Department, Mohammed 6 Polytechnic University (UM6P), Lot 660 – Hay Moulay Rachid, 43150, Benguerir

[2]Laboratoire Interdisciplinaire de Recherche des Sciences et Techniques, Faculté polydisciplinaire de Béni-Mellal, Université Sultan Moulay Slimane, BP 592, 23000 Béni-Mellal, Morocco.

[3]UR BIA 1268 Biopolymères Interactions Assemblages, INRA, 44316 Nantes, France

[4]IATE, CIRAD, Montpellier SupAgro, INRA, Université de Montpelier, 34060, Montpellier, France.

[*] E-mail: mounir.elachaby@um6p.ma; phone (+2126) 620 10 620

**Highlights**

- Cellulose nanocrystals (CNC) were successfully extracted from red algae waste
- CNC exhibit a needle-like shape and a diameter of 5-9 nm, and a length of 289-315 nm
- PVA nanocomposite films with different CNC contents were prepared by solvent-casting
- Nanocomposites with high mechanical performance and good transparency were obtaine

**Abstract**

Red algae is widely available around the world and its exploitation for the production of agar products has become an important industry in recent years. The industrial processing of red algae generates a large quantity of solid fibrous wastes, which constitutes a source of serious environmental problems. In the present work, the utilization of red algae waste as raw material to produce high-quality cellulose nanocrystals (CNC) has been investigated, and the ability of the as-isolated CNC to reinforce polymer has been studied. Red algae waste was chemically treated *via* alkali, bleaching and acid hydrolysis treatments, in order to obtain pure cellulose microfibers and CNC. The raw waste and the as-extracted cellulosic materials were successively characterized at different stages of treatments using serval analysis techniques. It was found that needle-like shaped CNC were successfully isolated at nanometric scale with diameters and lengths ranged from 5.2 ± 2.9 to 9.1 ± 3.1 nm, and from 285.4 ± 36.5 to 315.7 ± 30.3 nm, respectively, and the crystallinity index ranged from 81 to 87 %, depending on the hydrolysis time (30, 40 and 80 minutes). The as-extracted CNC were used as nanofillers for the production of polyvinyl alcohol (PVA)-based nanocomposite films with improved thermal and tensile properties, as well as optical transparency. It is shown that the addition of 8 wt % CNC into the PVA matrix increased the Young's modulus by 215 %, the tensile strength by 150 %, and the toughness by 45 %. Additionally, the nanocomposite films maintained the same transparency level of the neat PVA film (transmittance of ~90% in the visible region), suggesting that the CNC were dispersed at the nanoscale.

***Keywords***—Red algae waste, acid hydrolysis, cellulose nanocrystals, polymer composites

## 1. Introduction

Cellulose is one of the most abundant matter on the earth, and widely used for various industrial applications, due to its unique properties such as renewability, biodegradability, high tensile strength and stiffness, cost effectiveness, light weight and environmental benefits [1,2]. Since its discovery and isolation by Anselme Payen in 1838, the structure and properties of cellulose have been largely studied and highlighted in the literature [1,3]. Cellulose is naturally present in plants, marine animals, marine biomass, fungi, bacteria, and invertebrates, among others [2,4]. From lignocellulosic materials, cellulose can be extracted in the form of fibers. It is considered to be water-insoluble compound and can plays an important role in maintaining the structure of a plant cell wall [2,3].

Using top-down processes, cellulose can be extracted from cellulose-rich materials in various forms including fibers, microfibers, microfibrills, nanofibers and nanocrystals [2,4,5]. Cellulose nanocrystals (CNC) is the nanoscale form of cellulose which can be produced in various morphological shapes such as sphere-like, rod-like, ribbon-like, or needle-like shape, having a compact structure of ordered cellulose chains stabilized by inter and intra-molecular hydrogen bonding, which make very interesting solid crystalline nanoparticles with unique characteristics [6–9]. Starting from pure cellulose fibers, CNC can be extracted by various methods such as acid hydrolysis, TEMPO-mediated oxidation, mechanical disintegration and enzyme-assisted hydrolysis [5,10]. Among these methods, acid hydrolysis process represents the most effective method, where the cellulose fibers are subjected to concentrated acid to hydrolyze the amorphous domains of the cellulose chains and leave the crystalline domains unaltered [7]. In this context, the sulfuric acid has been extensively used for CNC extraction, however, hydrochloric, phosphoric and hydrobromic acids have also been reported for such purposes [3]. The sulfuric acid hydrolysis is a simple process and it requires shorter reaction time than other processes [2].

Additionally, this process produces CNC with functionalized surface, high crystallinity and good colloidal stability in water [3]. Unfortunately, this process has some drawbacks for large scale production, such as serious large water usage, equipment corrosion, and generation of huge amount of waste [5]. It should be noted that, the physico-chemical properties of CNC are strongly related to the nature of the bio-sourced raw materials and the hydrolysis conditions such as time, temperature, agitation and acid concentration [3,9].

Until recently CNC have been largely extracted from lignocellulosic materials (biomass containing cellulose, hemicellulose and lignin as the main substances) using various cellulose rich bio-sourced materials such as wood, straw, cotton, sisal, flax, ramie, bamboo pulp, coconut husk, rice husk, and sugarcane bagasse, among others [3,9]. More recently, CNC were successfully extracted from marine biomass such as posidonia oceanica ball and leaves [11,12] and Gelidium elegans [10]. Marine biomass, especially algae derivatives, contains low amounts of natural physicochemical barriers, making the cellulose accessible without a severe chemical treatment. It also contains a higher yield of carbohydrates and grows faster than typical terrestrial lignocellulosic biomass [10,13,14]. Marine biomass is, thus, considered to be a potential source for the production of cellulose fibers and its derivatives such as CNC.

Marine algae are categorized mostly into several main groups based on their photosynthetic pigmentation variations, i.e. green, blue-green, red, brown and golden algae [15]. There are about 55 000 kinds of algae species but only a dozen are commercially cultivated worldwide, with 27.1% of all known species of marine plants are red algae. Concerning chemical composition, red algae consist mostly of polysaccharides, small amounts of proteins, traces of lipids, and inorganic materials. The body of red algae contains large amounts of mucilaginous materials such as agar or carrageenan. The exploitation of red algae, especially *Gelidium sesquipedale*, for the production of agar products has become an important industry in recent years [16]. It generates a

large quantity of solid fibrous wastes which cause serious environmental problems [17]. Indeed, this algae waste (AW) is available in large amount and its valorization for the production of high value-added materials is not developed yet. However, the AW has been directly applied as soil conditioner and/or fertilizer in many coastal regions around the world [18–20], and can be reused as biosorbents for heavy metals [21,22]. After the extraction of Agar-Agar, the remaining AW mostly consists of 87.4 % of organic matter of which 31.60 % is made up of proteins and 54.95 % of total sugars, which include lignocellulosic fibers [17]. This renders AW a good bio-sourced material for the production of cellulose derivatives, such as highly crystalline CNC, for advanced composite materials development, which is the main objective of the present work.

The use of CNC as reinforcing fillers in polymer-based nanocomposites has attracted a lot of attention in the field of nanotechnology. It has been widely demonstrated that the incorporation of CNC into biopolymers can result in nanocomposite materials with high mechanical, optical, thermal, and barrier properties [23]. This is possible because of CNC's special morphology (generally needle like-shape), structure (ordered cellulose chains), large specific surface area (~250-500 $m^2/g$), low density, high crystallinity, high tensile strength (7.500 GPa), and very high elastic modulus (approximately 100-140 GPa) [7,9]. Additionally, CNC possess abundant hydroxyl groups on their surfaces, making them hydrophilic nanomaterials, which may facilitate their dispersions within water-soluble polymer matrices [7].

The aim of the current work is to explore the re-valorization of red algae waste (fibrous residue of red algae after extraction of agar-agar product) for the isolation of CNC using the same chemical treatments that are largely used for CNC isolation from typical terrestrial lignocellulosic materials, e.g. alkali, bleaching and sulfuric acid hydrolysis treatments [23–25]. CNC were extracted at various hydrolysis times (30, 40 and 80 min), in order to investigate the influence of extraction time on the yield, morphology, size, crystallinity, thermal stability of the resulting

CNC. This parameter was selected because it was identified as one of the most important parameters for obtaining CNC using the acid hydrolysis treatment [26–28]. After their successful extraction, the as-obtained CNC were successfully characterized in terms of their physico-chemical properties, and used as nanoreinforcing fillers for polymer nanocomposites development, using polyvinyl alcohol (PVA) as a polymeric matrix. PVA is a material with technological potential as a biodegradable polymer. It has wide commercial applications due to its unique chemical and physical properties. This polymer is nontoxic, highly crystalline, and water-soluble polymer that has good film-forming ability and hydrophilic properties, which arise from the presence of -OH groups on its macromolecular chains, which could be useful to link the functional groups of CNC, leading in the formation of hydrogen bonds. The PVA-CNC nanocomposites were produced thought solvent casting method and characterized regarding their thermal, transparency and mechanical properties.



## 2. Materials and experimental detail

### 2.1. Materials

Unpurified algae waste (AW) (Moisture = 9.11 %; ash = 14.13%), which is generated from industrial processing of agar-agar production, was provided by SETEXAM Company localized in Kenitra City in Morocco. The PVA polymer (Mw 31,000-50,000) and all the analytical grade chemicals used for extraction, bleaching, and hydrolysis were purchased from Sigma–Aldrich and used without further purification.

### 2.2. Production of cellulose fibers

CNC were successfully extracted from AW by alkali and bleaching treatments followed by an acid hydrolysis process, as described in our previous works [23,24,29]. The as-received AW samples were first cut into small pieces (≤ 2 cm), which were ground using a precision grinder

equipped with a 2 mm sieve screen (RETCH SM 100). The ground AW fibers were washed with distilled water for 1 hour at 60 °C under mechanical stirring. Then, the prewashed AW fibers were treated three times with a 4 wt% NaOH solution at 80 °C for 2 hours under stirring. The resulting alkali-treated algae waste (ATAW) was bleached 3 times at 80 °C for 2 h with a solution made up of equal parts (v:v) of acetate buffer (27 g NaOH and 75 mL glacial acetic acid, diluted to 1 L of distilled water) and aqueous sodium chlorite (1.7 wt% $NaClO_2$ in water), resulting in pure white colored cellulose fibers, defined as bleached algae waste (BAW). The overall steps of CNC extraction and digital images of each obtained products are presented in Figure 1.

### 2.3. Isolation of CNC

The as-produced bleached algae waste (BAW) was submitted to a sulfuric acid hydrolysis to isolate CNC. The acid hydrolysis was performed under mechanical stirring, using a 64 wt% sulfuric acid solution at 50 °C for three different hydrolysis times: 30, 40 and 80 minutes. Then, the mixture was diluted with ice cubes in order to stop the reaction and was washed by successive centrifugations at 12000 rpm at 15 °C for 20 minutes at each step and dialyzed against distillated water until it reached neutral pH. Afterward, the obtained CNC aqueous suspension was homogenized by the use of a probe-type ultrasonic homogenizer for 5 minutes in an ice bath. After that, CNC aqueous suspensions isolated at 30, 40 and 80 minutes were obtained in the form of white gels, as shown in Figure 1. Finally, a small quantity of the homogenized CNC suspension was freeze-dried to obtain the CNC in a solid form for characterizations (Figure 1). The CNC samples were coded $CNC_{30}$, $CNC_{40}$ and $CNC_{80}$, for CNC isolated at 30, 40 and 80 minutes, respectively.

### 2.4. Nanocomposite films processing

Using the solvent casting technique, the $CNC_{30}$ samples were used as nanoreinforcing fillers to produce PVA-CNC nanocomposite films, at different CNC contents (1, 3, 5 and 8 wt %). For each nanocomposite formulation (3 g of dry mass) a PVA solution was prepared by dissolving the desired amount of PVA powder in 40 ml of distilled water, while stirring for 1 h at 90 ° C. After cooling to room temperature, a CNC aqueous suspension containing the desired amount of CNC was added to the PVA solution. The mixture was then stirred for 1h at room temperature. The obtained PVA-CNC film-forming solution was sonicated for another 30 minutes. Finally, the PVA-CNC film-forming solution were casted into Petri dishes and the water evaporated at ambient temperature for 3 days. Neat PVA film was also prepared according to the same process mentioned above, without the addition of CNC. The PVA-CNC nanocomposite films were coded as PVA, PVA-CNC-1, PVA-CNC-3, PVA-CNC-5 and PVA-CNC-8. The number in each code name indicates the weight fraction of CNC in each nanocomposite formulation.

### 2.5. Characterization techniques

Zeta potential measurement of CNC suspension was measured using a Malvern Zetasizer Nano ZS instrument. For this measurement, a capillary cell was used and the CNC suspension was diluted and sonicated for 5 min before being analyzed. CHNS Elemental analysis for AW, ATAW, BAW and CNC samples was carried out on Elementar analysensysteme GmbH; Analyzer vario MICRO V4.0.2. The morphology and dimensions of the as-produced CNC were determined using Transmission Electron Microscopy (TEM) (Philips CM200 microscope). For each CNC sample ($CNC_{30}$, $CNC_{40}$ and $CNC_{80}$), a drop of a diluted suspension was deposited on the surface of a glow-discharged carbon-coated grid. To enhance the contrast, the CNC were negatively stained in a 2 wt% solution of uranyl acetate. The sample was dried at ambient

temperature before TEM analysis and the measurement was carried out with an accelerating voltage of 80 kV. Fourier Transform Infrared Spectroscopy (FTIR) of all studied samples were measured on a Tensor27 apparatus, the experiments were recorded in transmittance mode in the range of 4000-400 $cm^{-1}$ with a resolution of 4 $cm^{-1}$ and an accumulation of 16 scans. Thermogravimetric Analysis (TGA) (Mettler Toledo) for all samples was conducted under a nitrogen atmosphere between 25 and 700 °C, at a heating rate of 10 °C/min. X-ray diffraction (XRD) characterizations of samples were performed on a Bruker diffractometer D8 Advance using Cu-Kα radiation. The diffraction patterns were obtained at diffraction angles between 5 and 50 °, at room temperature. The crystallinity index (CrI%) of the samples was estimated following Segal's equation $CrI = \frac{I_{002} - I_{amorph}}{I_{002}} \times 100$ [30], where $I_{002}$ and $I_{amorph}$ are the peak intensities of crystalline and amorphous cellulose, respectively. Ultraviolet–visible (UV-vis) spectroscopy of the nanocomposite films was carried out using a Lambda 950 spectrophotometer. The film samples were placed directly in the spectrophotometer test cell, and the air was used as reference. The optical transmittance of films was measured in the wavelength range of 200–800 nm. Tensile tests were performed using a texture analyzer (TA.XT plus). The tensile specimens were cut in a rectangular shape with dimensions of 80 mm in length and 10 mm in width. The gauge length was fixed at 30 mm and the speed of the moving clamp was 5 mm/min. All tests were performed on a minimum of five samples and the reported results were averaged.

## 3. Results and discussions

### 3.1. Elemental analysis and Isolation of CNC

CNC at different times of hydrolysis (30, 40 and 80 minutes) were successfully isolated from red algae waste (AW), which is typically generated from the exploitation of raw marine red algae (Gelidium sesquipedale) for agar-agar extraction. The process and the physical aspect of

cellulosic materials obtained at different stages of treatment are summarized in Figure 1. Once the AW is dried and crushed, its color turns from an initial brown color to visually a yellow-brown, as shown in Figure 1. After washing with hot water, the ground AW fibers were subjected to an alkali treatment in order to eliminate the non-cellulosic compound (lignin, hemicellulose and pectin), which results in a yellow colored alkali-treated algae waste (ATAW) fibers (Figure 1). These ATAW fibers were partially dissociated due to the breakage of certain alkali-labile linkages between lignin monomers or between lignin and polysaccharides [24]. Next, ATAW fibers were subjected to a bleaching treatment in order to remove the lignin and impurities that remain after the alkaline treatment. The bleaching treatment may cause total defibrillation of the fibers in small microfibrils containing pure bleached cellulose, which can be identified by a very white color, indicating that the non-cellulosic compounds were probably eliminated by bleaching treatment (Figure 1). The yield of bleached algae waste (BAW) was calculate at 21.5 % with respect to the initial amount of starting unpurified AW.

Table 1 shows the results obtained from elemental analysis for AW, ATAW and BAW samples. It should be noted that all samples present high carbon and hydrogen contents, which is in accordance with the literature [17]. As stated below, AW is rich in organic matter, including proteins and sugars, which explains the high values of N, C and O (%). A removal of N (%) content in ATAW and BAW indicates a total elimination of proteins after alkali and bleaching treatments.

After bleaching, the BAW fibers were then subjected to a sulfuric acid hydrolysis, at different hydrolysis times (30, 40 and 80 minute), in order to remove the amorphous domains of cellulose chains. This resulted in CNC bundles with nanometric dimensions showing a high stability in water, as visually observed in Figure 1.

The stability of the CNC suspension can be deduced from the zeta potential measurement. Herein, the as produced $CNC_{30}$, $CNC_{40}$ and $CNC_{80}$ suspensions have a zeta potential of -25.17, -28.25 and -30.71 mV, respectively. It is seen that the increased hydrolysis time resulted in the insertion of large amount of negatively charged sulfate groups on the surface of CNC [26]. This finding was further confirmed by measuring the sulfate content (% S) of $CNC_{30}$, $CNC_{40}$ and $CNC_{80}$ from elemental analysis. Indeed, the % S measured for $CNC_{30}$, $CNC_{40}$ and $CNC_{80}$ was found to be 1.23 %, 1.47 % and 1.95 %, respectively, showing a proportionality between the zeta potential value and the amount of % S. All the obtained suspensions can be considered stable since the absolute value is greater than 25 mV [31]. Indeed, the good stability is caused by the exclusion of the polar components, the insertion of polar sulfate groups upon acid hydrolysis, and the exposure of the -OH groups from the cellulosic structure [29].

After separation from water by a freeze-drying process, clearly white powdered forms for $CNC_{30}$, $CNC_{40}$ and $CNC_{80}$ were obtained with a yield of about 13.76 %, 12.9 % and 11.18 %, respectively, with respect to the starting raw materials (AW). The decrease of the CNC yield with increasing of hydrolysis time has been previously reported for the extraction of CNC from raw cellulose-rich materials [26,27,32]. Comparatively, with regard to the starting raw materials, the yield of the as-isolated CNC was higher than that of the CNC isolated from rice straw (4.83–6.43%) [33], and red algae (Gelidium elegans) (8.07%) [10].

### 3.2. TEM observations of CNC

The morphology and dimensions of CNC samples ($CNC_{30}$, $CNC_{40}$ and $CNC_{80}$) were examined by TEM observations (Figure 2). These images clearly show that all the as-extracted

CNC have a needle-like morphology, thus confirming their successful extraction from AW. These results demonstrate the efficiency of the conditions used in the acid hydrolysis treatment and confirm that $CNC_{30}$, $CNC_{40}$ and $CNC_{80}$ aqueous suspensions contained individual nanocrystals. Noting that the morphology of CNC was not affected by increasing the hydrolysis time, indicating that the ordered cellulose chains were not degraded at high hydrolysis time (80 minutes).

The average diameter and length of all extracted CNC samples were determined by analyzing the high-magnification TEM images (Figure 2.a, c, e) using digital image analysis (Image J) [12], which confirmed that the CNC were extracted at nanometric scale. From this analysis, an average diameter of 9.1 ± 3.1, 7.6 ± 3.4 and 5.2 ± 2.9 nm, and an average length of 315.7 ± 30.3, 294.5 ± 29.1 and 285.4 ± 36.5 nm were measured for $CNC_{30}$, $CNC_{40}$ and $CNC_{80}$, respectively. It should be noted that longer hydrolysis times led to the isolation of smaller CNC in terms of their diameter and length. The same trend has been recently reported for CNC extracted from capim mombaça [32]. The aspect ratio of CNC is an important parameter, especially when CNC are intended as a nanoreinforcing fillers for polymer nanocomposites. In general, an aspect ratio greater than 13 promotes the formation of an anisotropic phase within the polymer matrix, thus resulting in nanocomposite materials with improved properties [34]. Herein, the average aspect ratio calculated for $CNC_{30}$, $CNC_{40}$ and $CNC_{80}$ samples was found to be 35, 42 and 57, respectively, indicating that as extracted CNC could be used as a dispersed phase for polymer nanocomposites development.

### 3.3. FTIR analysis of cellulosic materials

FTIR analysis of AW, ATAW, BAW and CNC ($CNC_{30}$, $CNC_{40}$ and $CNC_{80}$) samples are given in Figure 3. Commonly, the peaks at 3350-3250 $cm^{-1}$ and 1636 $cm^{-1}$ observed in all samples were attributed to the hydrogen bond of OH stretching and bending vibrations of the adsorbed water, which is related to the hydrophilic nature of cellulosic materials [10]. In addition, the peaks at 3350-3250 $cm^{-1}$ is also related to OH stretching vibration from cellulose molecules [2,35]. In all studied samples, the peak at 1157 $cm^{-1}$ is attributed to C-O-C asymmetric stretching of the cellulose [36]. Remarkably, the intensity of this peak was gradually increased from raw AW to CNC, indicating that the cellulose content was increased during different chemical treatments starting from AW and ending with extracted CNC.

Raw AW composed of protein, its FTIR spectrum shows a characteristic peak at 1520 $cm^{-1}$ which is associated with the stretching vibration of N-H band of the protein amide II structure [37]. Additionally, this peak is also associated to the C=C stretching from aromatic hydrocarbons of lignin [38]. However, this peak disappeared in bleached sample (BAW) and CNC spectra, which means the elimination of protein and lignin molecules after different chemical treatments. This result agrees well with elemental analysis result (Table 1) in which the % N content was totally removed after bleaching and acid hydrolysis processes. The peak observed at 1239 $cm^{-1}$ is attributed to the stretching vibration of the acyl-oxygen CO-OR, which is associated with the hemicellulose molecule [39]. However, this peak is absent in BAW and CNC samples, confirming that the hemicellulose is absent in these samples, as results of bleaching and acid hydrolysis treatments.

In all samples, the observed peaks at 1110 and 899 $cm^{-1}$ are associated with the presence of β-glucosidic ether linkages (C-O-C) related to the vibration modes of anhydro-glucopyranose ring skeleton, and to the β-glycosidic linkages between the anhydroglucose rings in the cellulose

chains [10]. These two prominent peaks are more intense in the case of BAW and CNC samples, indicating that more cellulose content was exposed in these samples after bleaching and acid hydrolysis treatments [40]. Additionally, the peak at 899 $cm^{-1}$ remained unchanged in all CNC samples ($CNC_{30}$, $CNC_{40}$ and $CNC_{80}$) indicating that the β-D-glucopyranosyl structure in cellulose chains was not affected after sulfuric acid hydrolysis, even at long hydrolysis time ($CNC_{80}$). Additionally, in the case of BAW and all CNC samples, the peaks observed at 1429, 1369 and 1312 $cm^{-1}$ were mainly associated with cellulose parent chain [41]. Based on these findings, it is evident that the bleached cellulose fibers and CNC were successfully isolated from raw AW, and the obtained results are in accordance with literature [10,41,42].

### 3.4. Thermogravimetric analysis of cellulosic materials

The thermal degradation behavior of AW, ATAW, BAW and CNC ($CNC_{30}$, $CNC_{40}$ and $CNC_{80}$) samples was investigated using thermogravimetric analysis. The obtained TGA/DTG curves of all samples are shown in Figure 4. Table 2 summarizes the onset temperature ($T_{onset}$) and the major maximum temperature ($T_m$) obtained from these curves. From these findings, all samples show a weight loss at temperatures lower than 100 °C, which is attributed to the moisture evaporation bonded on the surface and/or in inside of the cellulosic fibers [10,26,35].

For raw AW fibers, the onset temperature ($T_{onset}$) was observed at 210 °C and the corresponding major maximum temperature ($T_{max}$) was determined at 324 °C, which was attributed to the decomposition of all organic compounds, such as cellulose, lignin, hemicellulose and pectin, that are presented in raw AW sample [10,12,43]. The same trend was observe for the ATAW sample, showing almost the same $T_{onset}$ (212 °C) as in case of the AW sample (210 °C). The major $T_{max}$, however, showed a value that is 10 °C higher than that determined for AW. This indicates that some compounds (lignin, hemicellulose and pectin for example) were partially removed after alkali-treatment. For both AW and ATAW samples, it is noteworthy that another

degradation stage was started at around 650 °C, which is related to degradation of inorganic compounds such as silica and weddellite (mineral form of calcium oxalate) that are present in raw AW and still present in ATAW sample after alkali-treatment [10], as observed in XRD patterns for AW and ATAW samples (Figure 5).

Remarkably, the BAW sample shows a $T_{onset}$ of 234 °C and a major $T_{max}$ of 349 °C, which are 24 °C and 25 °C higher than those determined for the AW sample. This decomposition is due to degradation processes of cellulose, such as dehydration, decarboxylation, depolymerisation and decomposition of glycosyl units [35]. This result indicates that the bleaching treatment could eventually enhance the thermal stability of the bleached cellulose due to the total removal of non-cellulosic and mineral compounds [10]. These results agreed well with the XRD results (Figure 5), where the absence of peaks are related to the absence of mineral compounds in the bleached cellulose (BAW sample).

As shown in Figure 4, all extracted CNC samples exhibited lower $T_{onset}$ and $T_{max}$ compared to other cellulosic materials (AW, ATAW and BAW). This finding was expected since various studies have shown that the insertion of sulfate groups, during sulfuric acid hydrolysis, lowers the thermal stability of CNC [24,26]. The presence of sulfate groups on the surface of the CNC has a catalytic effect in the thermal decomposition mechanism [32], which results in a reduced thermal stability for sulfuric acid hydrolyzed CNC. It is noteworthy that the increase of hydrolysis time has a large effect on the $T_{onset}$ and the $T_{max}$ of the isolated CNC. Indeed, the $T_{onset}$ and $T_{max}$ were reduced from 201 °C and 231 °C for $CNC_{30}$ to 134 °C and 215 °C for $CNC_{80}$, respectively (Table 2). This result can be explained by percentage of sulfate groups present on the surface of CNC. As stated above, the elemental analysis shows that the percentage of sulfate content on the surface of CNC was increased with increasing of hydrolysis time, and thus the catalytic effect

was more pronounced in CNC containing high percentage of sulfate groups ($CNC_{80}$), in comparison to those containing low percentage of sulfate groups ($CNC_{30}$ and $CNC_{40}$), resulting in reduced thermal stability for CNC extracted at high hydrolysis time.

### 3.5. X-Ray diffraction analysis

The crystalline structure and the crystallinity index of all cellulosic samples are given in Figure 5. The XRD patterns show that the major peaks at 2θ values of around 14.8 °, 16.4°, 22.4°, which correspond to the (110), (11-0 ) and (002) planes [44], indicate the predominance of cellulose I in all samples (AW, ATAW, BAW, $CNC_{30}$, $CNC_{40}$ and $CNC_{80}$). It is noteworthy that the peaks observed at 2θ of 25-30 °, in AW and BAW samples, correspond to mineral impurities that are generally presented in sea biomass, such as silica ($SiO_2$) and weddeellite ($CaC_2O_4.2H_2O$) [12,45]. However, the absence of the XRD peaks in the bleached sample pattern (BAW) indicate that the mineral compounds were removed after the bleaching treatment (Figure 5).

The crystallinity index (*CrI*) of AW, ATAW, BAW and CNC ($CNC_{30}$, $CNC_{40}$ and $CNC_{80}$) samples was found to be 39 %, 53 %, 66 % and 81-87 % respectively, as determined from Segal's equation [30]. This finding indicates that the *CrI* of cellulosic samples improved during the chemical treatments. The increasing of *CrI* from the raw AW to the BAW sample was ascribed to the progressive removal of non-cellulosic compounds, as confirmed by FTIR analysis (Figure 3). Additionally, the *CrI* increased from 66 % for bleached sample to 81, 83 and 87 % for $CNC_{30}$, $CNC_{40}$ and $CNC_{80}$, respectively, indicating the removal of amorphous parts in the cellulose chains without destruction of the crystalline domains. It is noteworthy that the *CrI* of CNC increased with increasing of hydrolysis time, suggesting that the removal of amorphous parts of cellulose is more pronounced at long hydrolysis time, leading to an increase in *CrI* of CNC up to 87 %. Although the rod-like structures were maintained, supported by TEM

observations. Herein, the as-isolated CNC shows a high *CrI* (81-87%) compared with the CNC which were extracted from red algae (73%) [10], mulberry (73.4%) [46] , or sugarcane bagasse (77- 65 %) [23,24].

### 3.6. Processing of nanocomposites and FTIR analysis

It is well know that PVA is a water-soluble polymer and its treatment in water can easily be achieved due to its hydrophilic nature [25]. Furthermore, sulfuric acid hydrolyzed CNC exhibits free hydroxyl groups and have anionic sulfate groups inserted on their surfaces, which make them highly water dispersible nanomaterials (Figure 1). Accordingly, the mixture of PVA and CNC in water can be easily done in controlled conditions, enabling the formation of a homogeneous and stable CNC-filled PVA mixtures. By casting these latter on petri dishes and evaporating of water, films with high quality, smooth surface, good flexibility, and 80-µm-thick were produced, example of these films are presented in Figure 6.

In a polymeric nanocomposite material the interfacial compatibility and the miscibility between the involved compounds are important factors which define the structure and properties of the final nanocomposite material. Herein, both PVA and CNC contain hydroxyl groups, which can be involved in the formation of the hydrogen bonds between them. FTIR analysis was conducted to investigate eventual intermolecular interactions between macromolecular chains of PVA and the functional groups of CNC. Figure 7 illustrates the FTIR spectra of neat PVA and PVA-CNC nanocomposite films. It is well known that the hydroxyl band is sensitive to the hydrogen bonding and can be compelled to a shifted wave number in FTIR spectra [47]. Remarkably, the addition of CNC into the PVA matrix resulted in a shifting of the hydroxyl bands in the range of 3500–3000 $cm^{-1}$ (3295 $cm^{-1}$ for PVA and 3283-3277 $cm^{-1}$for PVA-CNC), indicating the existence of hydrogen bonding interactions between the hydroxyl groups on the surface of CNC and the hydroxyl groups on the macromolecular chains of PVA polymer. Similar

trends have been reported for CNC-filled PVA/Chitosan blend [23], CNC-filled PVA [48], and graphene oxide-filled PVA nanocomposite films [47].

### 3.7. Thermal stability

The TGA measurement is considered the best method for studying the thermal stability and degradation of polymer-based systems. Herein, the thermal stability of the PVA-CNC nanocomposite was studied in a nitrogen atmosphere. Figure 8 shows the TGA and DTG curves of neat PVA and PVA-CNC nanocomposites. It should be noted that all TGA/DTG curves exhibit three noticeable mass loss steps, with three maximum temperature peaks at around 110 °C, 331 °C and 435 °C. This can be explained as the stepwise decomposition and degradation processes of the PVA macromolecules beginning from evaporation of adsorbed moisture and lasting to the absolute ash formation. All decomposition processes of neat PVA and its nanocomposites end below 500 C°. From TGA/DTG curves, the moisture content (MC, weight loss at around 100 °C), the onset temperature ($T_{onset}$, beginning of weight loss at around 180-220 °C), the temperature corresponding to a weight loss of 10% ($T_{10\%}$), and the residual weight (RW) were obtained and summarized in Table 3. It is clear that the moisture content and the onset temperature were affected by the addition of CNC. Indeed, the moisture content was reduced from 6.27 % for neat PVA to 4.06 for PVA nanocomposite containing 8 wt% CNC, this might be explained by the interaction between both phases (PVA and CNC) *via* hydrogen bonds, which lead to the reduction of the number of free hydroxyl groups that gives the hydrophilic character to PVA polymer matrix and CNC nanofillers, and thus a decrease of moisture uptake with increasing of CNC content in nanocomposite systems [49]. The $T_{onset}$ and $T_{10\%}$ (temperature corresponding to a weight loss of 10 %) were gradually increased with increasing CNC content. Indeed, the $T_{onset}$ and $T_{10\%}$ determined for PVA nanocomposite containing 8 wt% CNC are 22.18 °C and 16.19 °C higher than those observed for neat PVA (188.74 °C and 272.12 °C),

respectively. This trend is attributed to the restriction of the mobility of polymer chains at the interfaces between the PVA and the CNC surfaces, improving in turn the thermal stability of PVA-CNC nanocomposite films. The measured residual weight (RW) was found to be identical for all samples (4.89-5.11 %), suggesting that the addition of CNC has not influenced the formation of the char residue.

### 3.8. Transparency properties of films

The local dispersion of CNC within PVA matrix and the transparency level of the resulting nanocomposite films were evaluated using UV–Vis spectroscopy. Figure 9 shows the UV-Vis transmittance spectra and its values at $\lambda$ = 700 nm of neat PVA and PVA-CNC nanocomposite films. It is well know that the PVA is a transparent polymer (92.37 % at $\lambda$ = 700 nm) and has good film forming properties that enable it to be used as polymeric matrix in nanocomposites development for advanced applications [48]. The transparency level of the PVA polymer was not largely affected by the addition of different CNC contents. Indeed, when the CNC content varied from 1 to 8 wt%, the UV-Vis transmittance of the resulting PVA nanocomposite was measured in the range of 83-93 % ; which is due to the nanoscale dispersion of CNC within the PVA matrix [23]. This behavior confirms that CNC have a good compatibility with the PVA polymer matrix which helps to avoid CNC aggregation, thus reducing the amount of light scattering and favoring the transmittance of visible light through the films. Indeed, a good transparency level for polymer-based nanocomposite films is an important property required for some advanced applications such as food packaging materials [50].

### 3.9. Tensile properties of bio-nanocomposite films

The improvement of tensile properties of polymer based nanocomposite materials are strongly related to the aspect ratio, the dispersion state and the intrinsic mechanical characteristics of the reinforcing nanofillers. Herein, the CNC ($CNC_{30}$) used as dispersed nanofillers have a relatively high aspect ratio (35) and present a good interfacial compatibility with polymeric chains, confirming their good dispersion/distribution within PVA polymer. Additionally, it is well know that CNC have a relatively high elastic modulus, which is approximatively measured at 100-150 GPa [7,9]. Based on these key points, the addition of CNC into PVA polymer should have a significant reinforcing impact on the tensile properties of the resulting nanocomposite films.

The tensile behavior of PVA-CNC nanocomposite films was characterized by uni-axial tensile tests. Typical stress-strain curves of all nanocomposite films at different CNC contents are presented in Figure 10. In order to evaluate the strength, the flexibility, and the stiffness of these nanocomposite films, the tensile modulus, tensile strength, elongation at break and toughness were extracted from the stress-strain curves and plotted in Figure 11 and as a function of the CNC content; and the values of these selected properties are summarized in Table 4.

The Young's modulus (Figure 11.a) can be defined as the slope of the linear elastic deformation of the stress–strain curve, the ultimate tensile strength (Figure 11.b) represents the maximum stress value applied to the material, the elongation at break (Figure 11.c) is defined as the strain to break the material, and the toughness (Figure 11.d) is the energy needed to break the material, and can be calculated from the area under the stress–strain curve [24].

From these data, it could be seen that all nanocomposites containing CNC exhibited superior tensile properties than those observed for neat PVA polymer, thus confirming that the addition of CNC has a positive effect on the improvement of the nanocomposite films' tensile properties. The neat PVA film exhibits an elastic modulus of 933.35 MPa, an ultimate tensile strength of 37.36 MPa, an elongation at break of 90.07 %, and a toughness of $24.43\times10^{8}$ $J.m^{-3}$. Nanocomposite films containing 8 wt% CNC (PVA-CNC-8) exhibit a Young's modulus of 2939.35 MPa, an ultimate tensile strength of 93.56 MPa and a toughness of $35.34\times10^{8}$ $J.m^{-3}$, which correspond to 215 %, 150 % and 45 % increases, respectively, in comparison with the neat PVA. These findings were previously observed for various CNC filled polymer nanocomposites [23,24,29]. Meanwhile, the elongation at break was reduced to 41.72 %, which corresponds to a 54 % decrease in comparison with neat PVA (90.07 %). This is also observed in a variety of previously reported CNC filled polymer nanocomposite, which is related to the reinforcing ability of rigid nanoparticles [23,24,29].

The improvement of the mechanical properties is attributed to the strong interfacial interactions between the PVA chains and CNC, which is due to the high contact area exposed on the CNC and their functionalized surfaces. During the processing of nanocomposite films, the original hydrogen bonds formed between the PVA chains were probably replaced by new hydrogen bonds formed between the hydroxyl groups that are presented on the surface of CNC as well as in PVA chains, thus resulting in efficient load transfer. The existence of these hydrogen bonds improved the tensile properties of the resulting PVA-CNC nanocomposite films. Such improvements confirmed that the PVA-CNC nanocomposite films have high strength and stiffness, which are the main mechanical properties required for advanced applications of nanocomposite materials.

## 4. Conclusion

In this work, high crystalline cellulose nanocrystals (CNC) have been successfully isolated from red algae waste *via* alkalization, bleaching and acid hydrolysis treatments. After their characterizations, the as-produced CNC were used as nano-reinforcing fillers for nanocomposites development. For this purpose, different CNC mass fractions (1, 3, 5 and 8 wt %) were dispersed into PVA matrix to produce PVA-CNC nanocomposite films, using solvent casting method. The results of the physicochemical characterization showed that the CNC samples have a crystallinity index of 81-87 %, an average diameter ranging from 5.2 ± 2.9 to 9.1 ± 3.1 nm, and an average length ranging from 285.4 ± 36.5 to 315.7 ± 30.3 nm, giving rise to an aspect ratio of 35-57, depending on the hydrolysis time. Their incorporation into the PVA polymer has shown a positive effect on the properties of the resulting nanocomposite films. The PVA-CNC nanocomposites exhibit improved tensile properties. By adding 8 wt % CNC into a PVA matrix, Young's modulus, tensile strength and toughness were increased by 215 %, 150 % and 45 % increases, respectively, in comparison to neat PVA. In addition, PVA-CNC nanocomposite films show a high level of optical transparency, confirming that the CNC was dispersed at the nanoscale. The improvement of the properties of the nanocomposite films is due to strong interfacial interactions generated by the hydrogen bond between the hydroxyl groups in the CNC and the PVA polymer.

This work was carried out in order to i) explore the reuse of red algae waste for the production of high crystalline nanoscaled cellulose crystals, ii) study their ability to strengthen the polymer matrices, and iii) produce new PVA-CNC nanocomposite films with good thermal, transparency and mechanical properties. The resulting nanocomposite films with superior properties are therefore excellent candidates for use in food packaging applications.

**Acknowledgment**

The financial assistance of the Office Chérifien des Phosphates (OCP S.A.) in the Moroccan Kingdom toward this research is hereby acknowledged. The authors would like to acknowledge SETEXAM Company in Morocco for providing us the raw Algal waste. This work was performed as part of a collaboration between the INRA of Montpellier and the Materials Science and Nanoengineering department (MSN) of the Mohamed 6 Polytechnic University (UM6P) in Morocco. The authors would like to thank Pr. Jones Alami, head of MSN Department of UM6P, for his help to improve this work.

**References**

[1] H. Tian, J. He, Cellulose as a Scaffold for Self-Assembly: From Basic Research to Real Applications, Langmuir. 32 (2016) 12269–12282.

[2] D. Trache, M.H. Hussin, C.T. Hui Chuin, S. Sabar, M.R.N. Fazita, O.F.A. Taiwo, T.M. Hassan, M.K.M. Haafiz, Microcrystalline cellulose: Isolation, characterization and bio-composites application—A review, Int. J. Biol. Macromol. 93 (2016) 789–804.

[3] Y. Habibi, L.A. Lucia, O.J. Rojas, Cellulose nanocrystals: Chemistry, self-assembly, and applications, Chem. Rev. 110 (2010) 3479–3500.

[4] I.A. Sacui, R.C. Nieuwendaal, D.J. Burnett, S.J. Stranick, M. Jorfi, C. Weder, E.J. Foster, R.T. Olsson, J.W. Gilman, Comparison of the properties of cellulose nanocrystals and cellulose nanofibrils isolated from bacteria, tunicate, and wood processed using acid, enzymatic, mechanical, and oxidative methods, ACS Appl. Mater. Interfaces. 6 (2014) 6127–6138.

[5] D. Trache, M.H. Hussin, M.K.M. Haafiz, V.K. Thakur, Recent progress in cellulose nanocrystals: sources and production, Nanoscale. 9 (2017) 1763–1786.

[6] G.H.D. Tonoli, E.M. Teixeira, A.C. Corrêa, J.M. Marconcini, L.A. Caixeta, M.A. Pereira-Da-Silva, L.H.C. Mattoso, Cellulose micro/nanofibres from Eucalyptus kraft pulp:

Preparation and properties, Carbohydr. Polym. 89 (2012) 80–88.

[7] N. Grishkewich, N. Mohammed, J. Tang, K.C. Tam, Recent advances in the application of cellulose nanocrystals, Curr. Opin. Colloid Interface Sci. 29 (2017) 32–45.

[8] D. Klemm, F. Kramer, S. Moritz, T. Lindstr??m, M. Ankerfors, D. Gray, A. Dorris, Nanocelluloses: A new family of nature-based materials, Angew. Chemie - Int. Ed. 50 (2011) 5438–5466.

[9] J. Tang, J. Sisler, N. Grishkewich, K.C. Tam, Functionalization of cellulose nanocrystals for advanced applications, J. Colloid Interface Sci. 494 (2017) 397–409.

[10] Y.W. Chen, H.V. Lee, J.C. Juan, S.M. Phang, Production of new cellulose nanomaterial from red algae marine biomass Gelidium elegans, Carbohydr. Polym. 151 (2016) 1210–1219.

[11] F. Bettaieb, R. Khiari, A. Dufresne, M.F. Mhenni, M.N. Belgacem, Mechanical and thermal properties of Posidonia oceanica cellulose nanocrystal reinforced polymer, Carbohydr. Polym. 123 (2015) 99–104.

[12] F. Bettaieb, R. Khiari, M.L. Hassan, M.N. Belgacem, J. Bras, A. Dufresne, M.F. Mhenni, Preparation and characterization of new cellulose nanocrystals from marine biomass Posidonia oceanica, Ind. Crops Prod. 72 (2015) 175–182.

[13] L. Korzen, N. Pulidindi, A. Israel, A. Abelson, A. Gedanken, RSC Advances Single step production of bioethanol from the seaweed Ulva rigida using sonication, RSC Adv. 5 (2015) 16223–16229.

[14] H.M. Kim, S.G. Wi, S. Jung, Y. Song, H.J. Bae, Efficient approach for bioethanol production from red seaweed Gelidium amansii, Bioresour. Technol. 175 (2015) 128–134.

[15] S. V. Vassilev, C.G. Vassileva, Composition, properties and challenges of algae biomass for biofuel application: An overview, Fuel. 181 (2016) 1–33.

[16] S. Yarnpakdee, S. Benjakul, P. Kingwascharapong, Physico-chemical and gel properties of agar from Gracilaria tenuistipitata from the lake of Songkhla, Thailand, Food Hydrocoll. 51 (2015) 217–226.

[17] K. and E. Ennouali, M., Ouhssine, M., Ouhssine, Biotransformation of algal waste by biological fermentation, African J. Biotechnol. 5 (2006) 1233–1237.

[18] H. Castlehouse, C. Smith, A. Raab, C. Deacon, A.A. Meharg, J. Feldmann, Biotransformation and accumulation of arsenic in soil amended with seaweed, Environ. Sci. Technol. 37 (2003) 951–957.

[19] C. Cocozza, A. Parente, C. Zaccone, C. Mininni, P. Santamaria, T. Miano, Comparative management of offshore posidonia residues: Composting vs. energy recovery, Waste Manag. 31 (2011) 78–84.

[20] S.F.I. Haslam, D.W. Hopkins, Physical and biological effects of kelp (seaweed) added to soil, Appl. Soil Ecol. 3 (1996) 257–261.

[21] V.J.P. Vilar, C.M.S. Botelho, R.A.R. Boaventura, Equilibrium and kinetic modelling of Cd(II) biosorption by algae Gelidium and agar extraction algal waste, Water Res. 40 (2006) 291–302.

[22] T.A. Davis, B. Volesky, R.H.S.F. Vieira, Sargassum seaweed as biosorbent for heavy metals, Water Res. 34 (2000) 4270–7278.

[23] N. El Miri, K. Abdelouahdi, A. Barakat, M. Zahouily, A. Fihri, A. Solhy, M. El Achaby, Bio-nanocomposite films reinforced with cellulose nanocrystals: Rheology of film-forming solutions, transparency, water vapor barrier and tensile properties of films, Carbohydr. Polym. 129 (2015) 156–167.

[24] N. El Miri, K. Abdelouahdi, M. Zahouily, A. Fihri, A. Barakat, A. Solhy, M. El Achaby, Bio-nanocomposite films based on cellulose nanocrystals filled polyvinyl alcohol/chitosan

polymer blend, J. Appl. Polym. Sci. 132 (2015) 1–13.

[25] N. El Miri, M. El Achaby, A. Fihri, M. Larzek, M. Zahouily, K. Abdelouahdi, A. Barakat, A. Solhy, Synergistic effect of cellulose nanocrystals/graphene oxide nanosheets as functional hybrid nanofiller for enhancing properties of PVA nanocomposites, Carbohydr. Polym. 137 (2016) 239–248.

[26] H. Kargarzadeh, I. Ahmad, I. Abdullah, A. Dufresne, S.Y. Zainudin, R.M. Sheltami, Effects of hydrolysis conditions on the morphology, crystallinity, and thermal stability of cellulose nanocrystals extracted from kenaf bast fibers, Cellulose. 19 (2012) 855–866.

[27] E. de M. Teixeira, T.J. Bondancia, K.B.R. Teodoro, A.C. Corrêa, J.M. Marconcini, L.H.C. Mattoso, Sugarcane bagasse whiskers: Extraction and characterizations, Ind. Crops Prod. 33 (2011) 63–66.

[28] H.A. Silvério, W.P. Flauzino Neto, N.O. Dantas, D. Pasquini, Extraction and characterization of cellulose nanocrystals from corncob for application as reinforcing agent in nanocomposites, Ind. Crops Prod. 44 (2013) 427–436.

[29] M. El Achaby, N. El Miri, A. Aboulkas, M. Zahouily, E. Bilal, A. Barakat, A. Solhy, Processing and properties of eco-friendly bio-nanocomposite films filled with cellulose nanocrystals from sugarcane bagasse, Int. J. Biol. Macromol. 96 (2017) 340–352.

[30] L. Segal, L. Creely, A.E. Martin, C.M. Conrad, An empirical method for estimating the degree of crystallinity of native cellulose using the X-ray diffrac- tometer, Text. Res. J. 29 (1959) 786–794.

[31] J.P.S. Morais, M.D.F. Rosa, M.D.S.M. De Souza Filho, L.D. Nascimento, D.M. Do Nascimento, A.R. Cassales, Extraction and characterization of nanocellulose structures from raw cotton linter, Carbohydr. Polym. 91 (2013) 229–235.

[32] D.F. Martins, A.B. de Souza, M.A. Henrique, H.A. Silvério, W.P. Flauzino Neto, D.

Pasquini, The influence of the cellulose hydrolysis process on the structure of cellulose nanocrystals extracted from capim mombaça (Panicum maximum), Ind. Crops Prod. 65 (2015) 496–505.

[33] P. Lu, Y.-L. Hsieh, Preparation and characterization of cellulose nanocrystals from rice straw, Carbohydr. Polym. 87 (2012) 564–573.

[34] A. Dufresne, Nanocellulose: From Nature to High Performance Tailored Materials, in W. De Gruyter GmbH, Berlin/Boston 2012, pp. 277–320.

[35] D. Trache, A. Donnot, K. Khimeche, R. Benelmir, N. Brosse, Physico-chemical properties and thermal stability of microcrystalline cellulose isolated from Alfa fibres, Carbohydr. Polym. 104 (2014) 223–230.

[36] K. Saelee, N. Yingkamhaeng, T. Nimchua, P. Sukyai, An environmentally friendly xylanase-assisted pretreatment for cellulose nanofibrils isolation from sugarcane bagasse by high-pressure homogenization, Ind. Crops Prod. 82 (2016) 149–160.

[37] A. Dmytryk, A. Saeid, K. Chojnacka, Biosorption of microelements by Spirulina: towards technology of mineral feed supplements, ScientificWorldJournal. 2014 (2014) 356328.

[38] Y.C. Ching, T.S. Ng, Effect of Preparation Conditions on Cellulose from Oil Palm Empty Fruit Bunch Fiber, BioResources. 9 (2014) 6373–6385.

[39] M.A. Mohamed, W.N.W. Salleh, J. Jaafar, S.E.A.M. Asri, A.F. Ismail, J.M. Kenny, L. Torre, H. Xiaojun, G. Xushan, Physicochemical properties of “green” nanocrystalline cellulose isolated from recycled newspaper, RSC Adv. 5 (2015) 29842–29849.

[40] D. Trache, K. Khimeche, A. Donnot, R. Benelmir, FTIR spectroscopy and X-ray powder diffraction characterization of microcrystalline cellulose obtained from alfa fibers, MATEC Web of Conferences. 3 (2013) 1023.

[41] Y.W. Chen, H.V. Lee, S.B. Abd Hamid, Preparation and Characterization of Cellulose

Crystallites via Fe(III)-, Co(II)- and Ni(II)-Assisted Dilute Sulfuric Acid Catalyzed Hydrolysis Process, J. Nano Res. 41 (2016) 96–109.

[42] X.Y. Tan, S.B. Abd Hamid, C.W. Lai, Preparation of high crystallinity cellulose nanocrystals (CNCs) by ionic liquid solvolysis, Biomass and Bioenergy. 81 (2015) 584–591.

[43] S. Thambiraj, D. Ravi Shankaran, Preparation and physicochemical characterization of cellulose nanocrystals from industrial waste cotton, Appl. Surf. Sci. 412 (2017) 405–416.

[44] D. Trache, K. Khimeche, A. Mezroua, M. Benziane, Physicochemical properties of microcrystalline nitrocellulose from Alfa grass fibres and its thermal stability, J. Therm. Anal. Calorim. 124 (2016) 1485–1496.

[45] F. Bettaieb, R. Khiari, A. Dufresne, M.F. Mhenni, J.L. Putaux, S. Boufi, Nanofibrillar cellulose from Posidonia oceanica: Properties and morphological features, Ind. Crops Prod. 72 (2015) 97–106.

[46] R. Li, J. Fei, Y. Cai, Y. Li, J. Feng, J. Yao, Cellulose whiskers extracted from mulberry: A novel biomass production, Carbohydr. Polym. 76 (2009) 94–99.

[47] J. Li, L. Shao, L. Yuan, Y. Wang, A novel strategy for making poly(vinyl alcohol)/reduced graphite oxide nanocomposites by solvothermal reduction, Mater. Des. 54 (2014) 520–525.

[48] E. Fortunati, D. Puglia, F. Luzi, C. Santulli, J.M. Kenny, L. Torre, Binary PVA bio-nanocomposites containing cellulose nanocrystals extracted from different natural sources: Part I, Carbohydr. Polym. 97 (2013) 825–836.

[49] M.-C. Popescu, Structure and sorption properties of CNC reinforced PVA films, Int. J. Biol. Macromol. 101 (2017) 783–790.

[50] J.-W. Rhim, H.-M. Park, C.-S. Ha, Bio-nanocomposites for food packaging applications,

Prog. Polym. Sci. 38 (2013) 1629-1652.

Figures

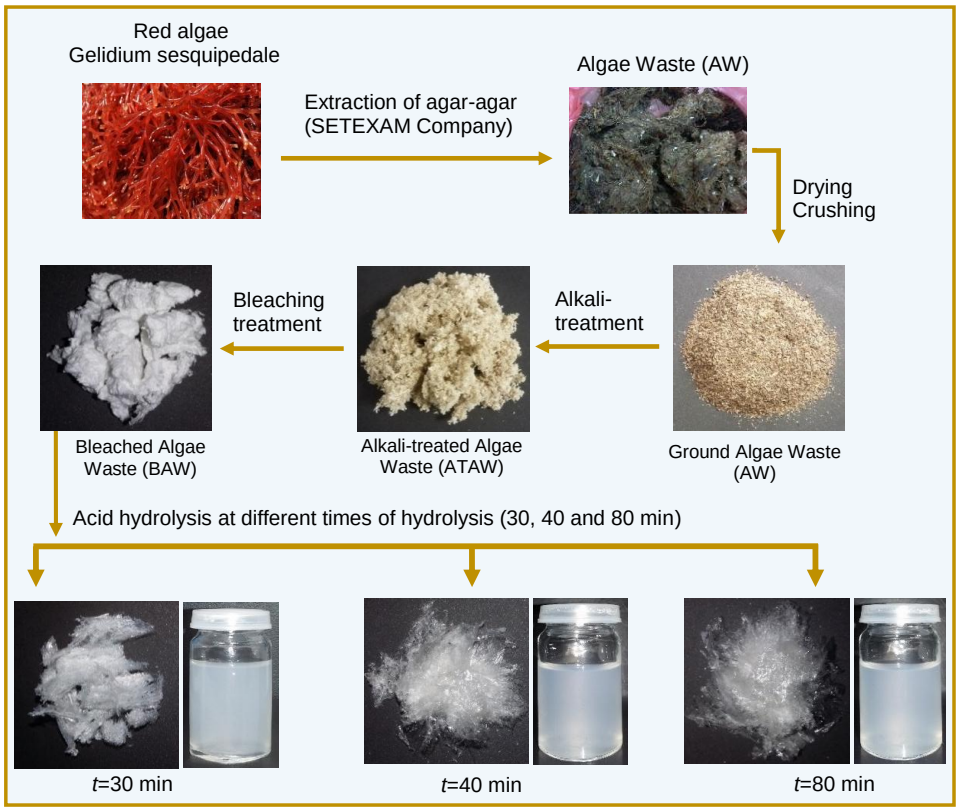


**Figure 1**: Overall steps of CNC extraction at different hydrolysis times and digital images of each obtained products

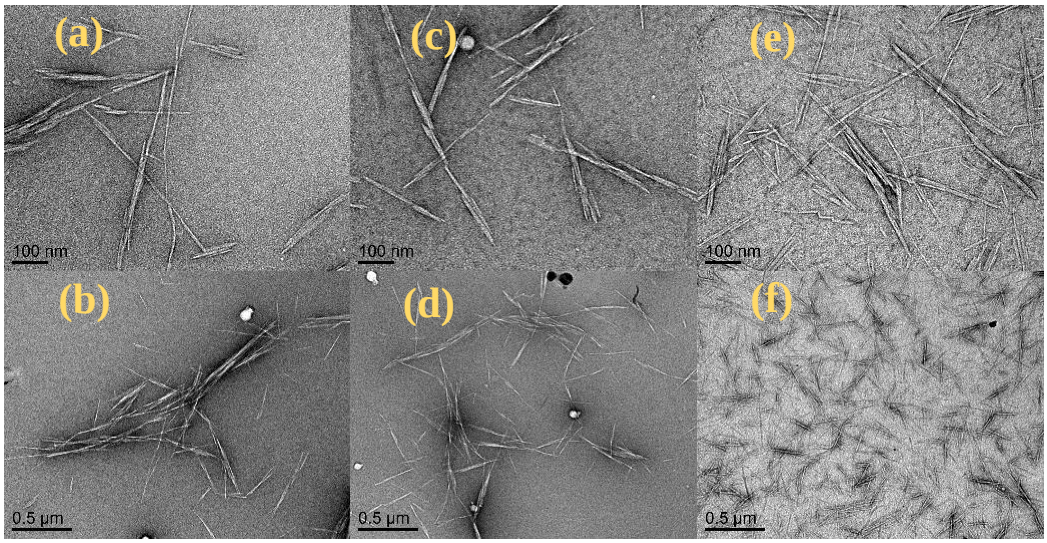


| Sample | D (nm) | L (nm) | L/D |
|---|---|---|---|
| $CNC_{30}$ | 9 ± 3.1 | 315 ± 30.3 | 35 |
| $CNC_{40}$ | 7 ± 3.4 | 294 ± 29.1 | 42 |
| $CNC_{80}$ | 5 ± 2.9 | 285 ± 36.5 | 57 |

**Figure 2:** TEM images of (a,b) $CNC_{30}$, (c,d) $CNC_{40}$ and (e,f) $CNC_{80}$ and their average diameter (D), length (L) and aspect ratio (L/D)

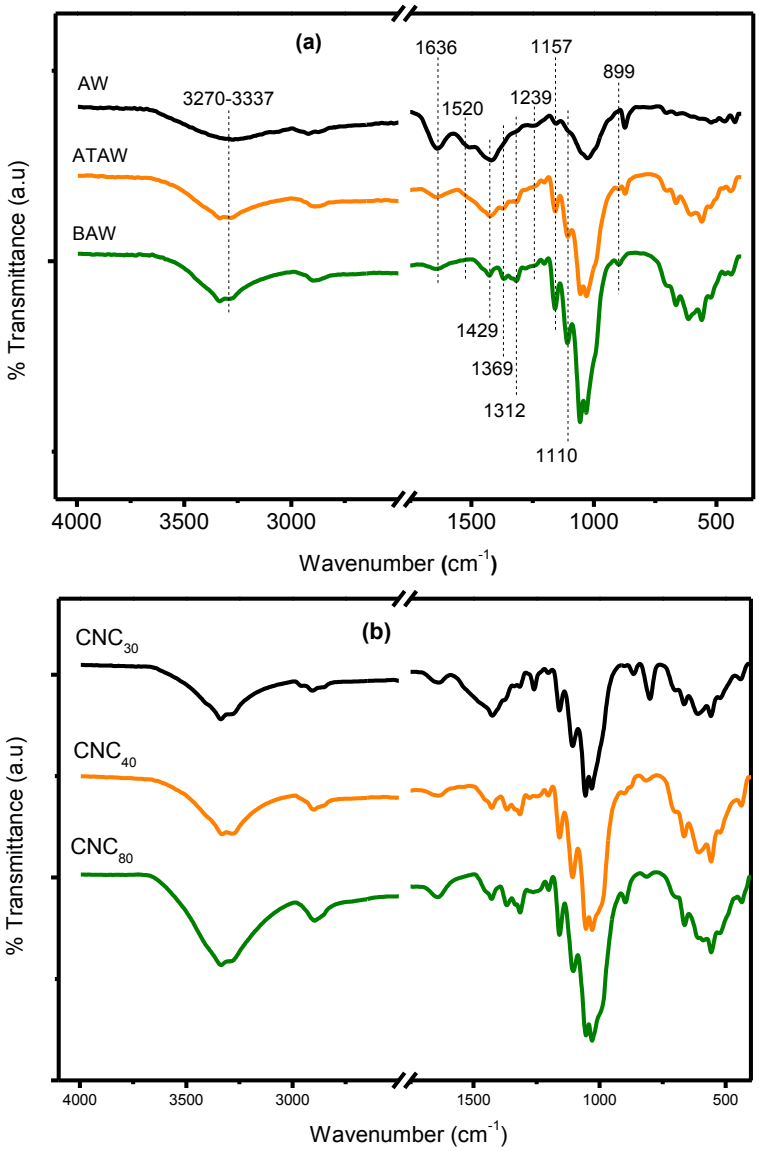


**Figure 3:** (a) FTIR spectra of ARBR, ARTA and ARBC samples and (b) FTIR spectra of $CNC_{30}$, $CNC_{40}$ and $CNC_{80}$ samples

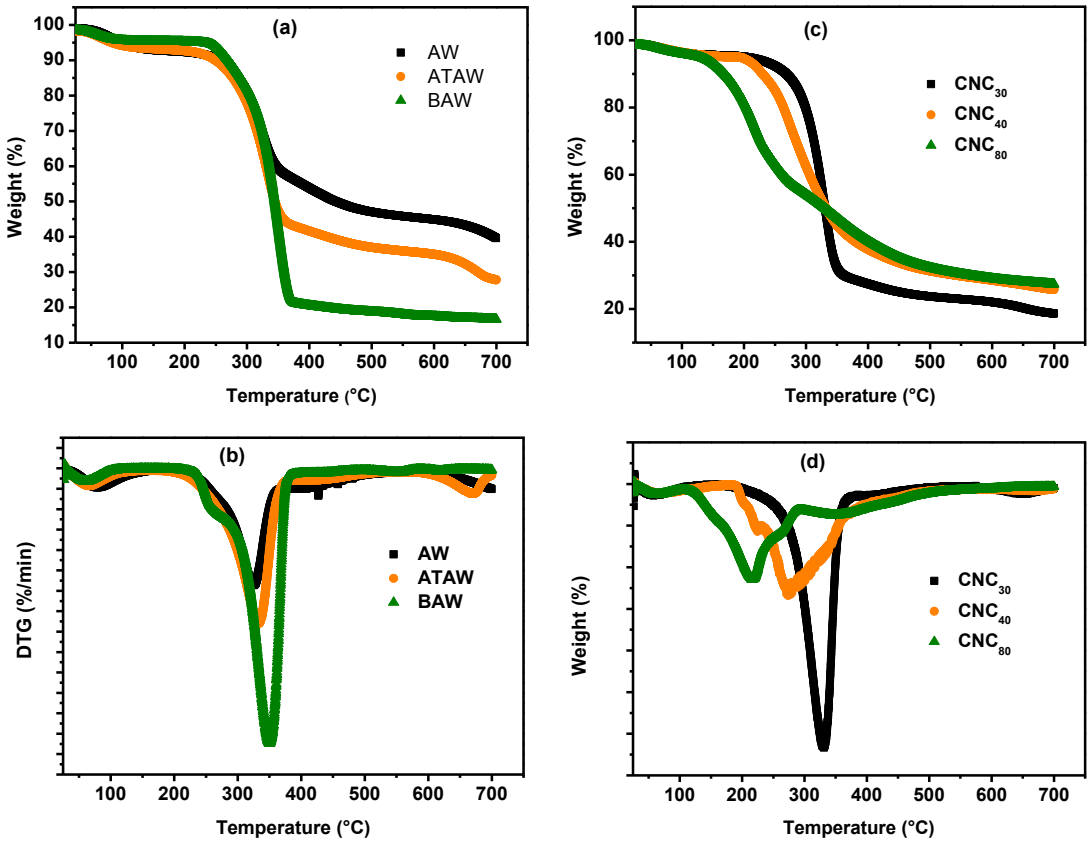


**Figure 4:** (a) TGA and (b) DTG curves of AW, ATAW and BAW samples and (c) TGA and (d) DTG curves of $CNC_{30}$, $CNC_{40}$ and $CNC_{80}$ samples.

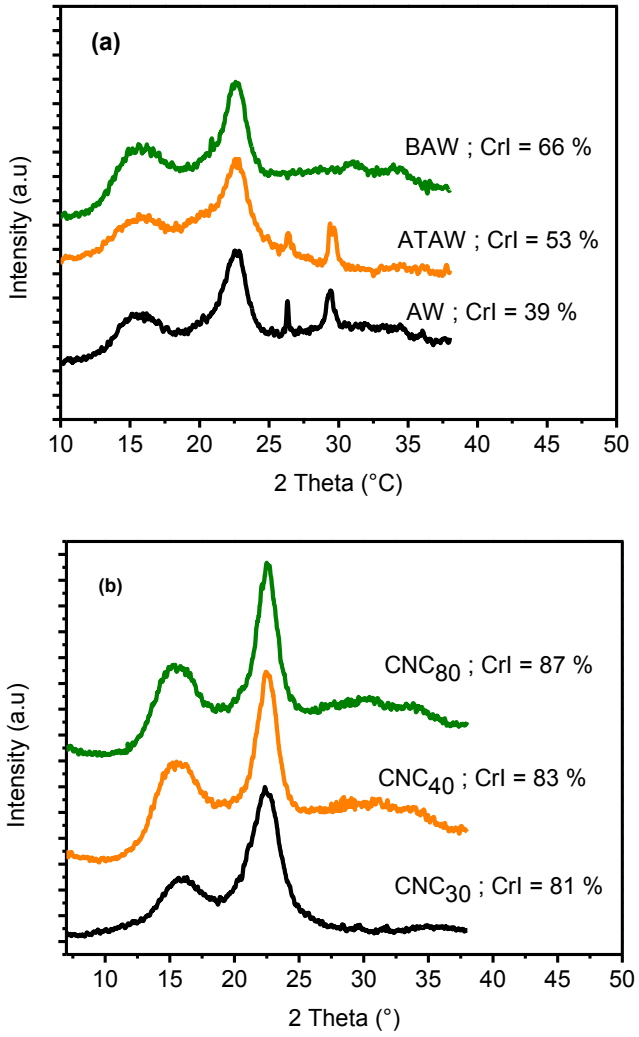


**Figure 5:** (a) XRD patterns of AW, ATAW and BAW samples and (b) XRD patterns of $CNC_{30}$, $CNC_{40}$ and $CNC_{80}$ samples

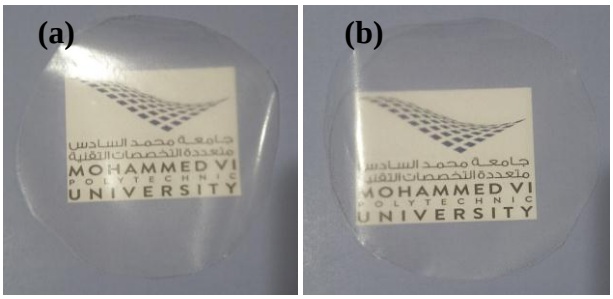


**Figure 6**: Examples of as-produced films with (a) neat PVA and (b) PVA-CNC-8 nanocomposite film

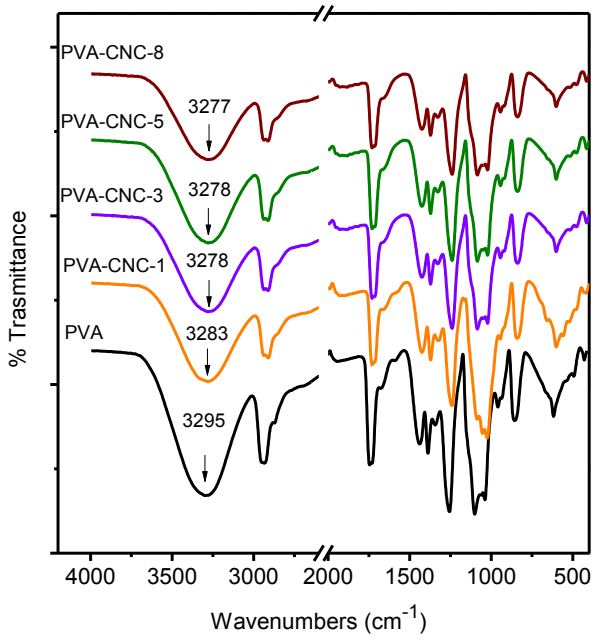


**Figure 7**: FTIR spectra of neat PVA and its nanocomposites

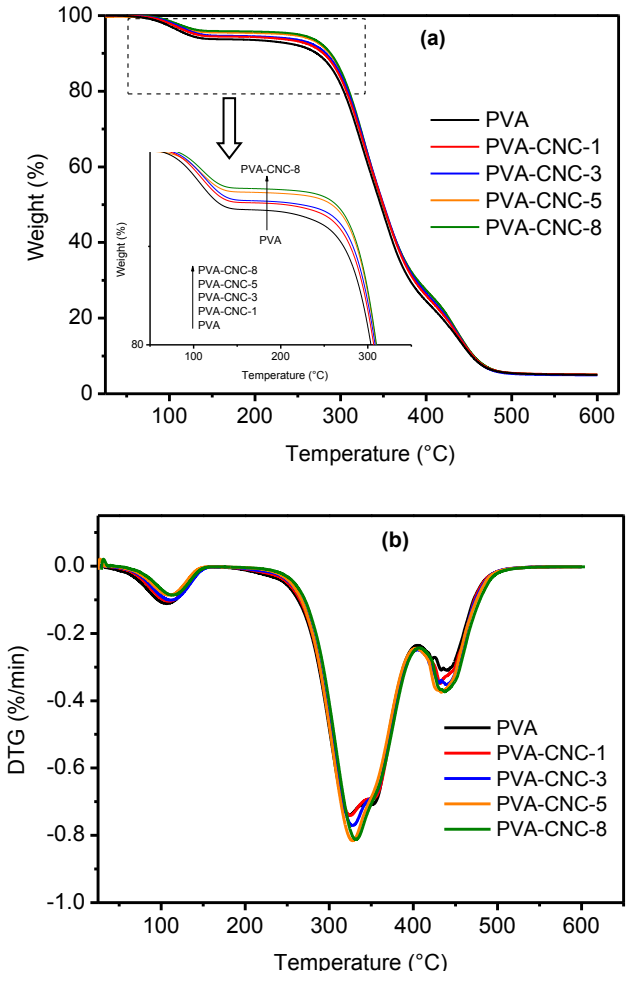

**Figure 8**: (a) TGA and (b) DTG curves of neat PVA and PVA-CNC nanocomposite films.

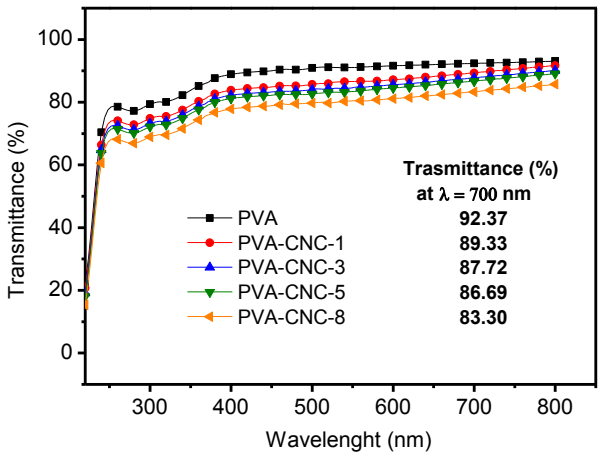


**Figure 9**: UV-Vis transmittance of neat PVA and its PVA-CNC nanocomposite films

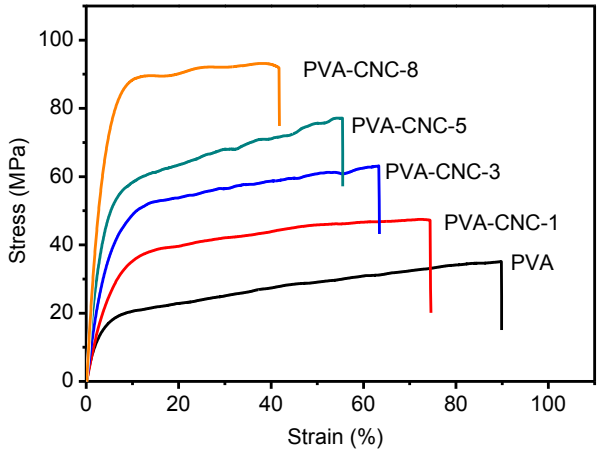


**Figure 10**: Typical stress-strain curves of neat PVA and its nanocomposites

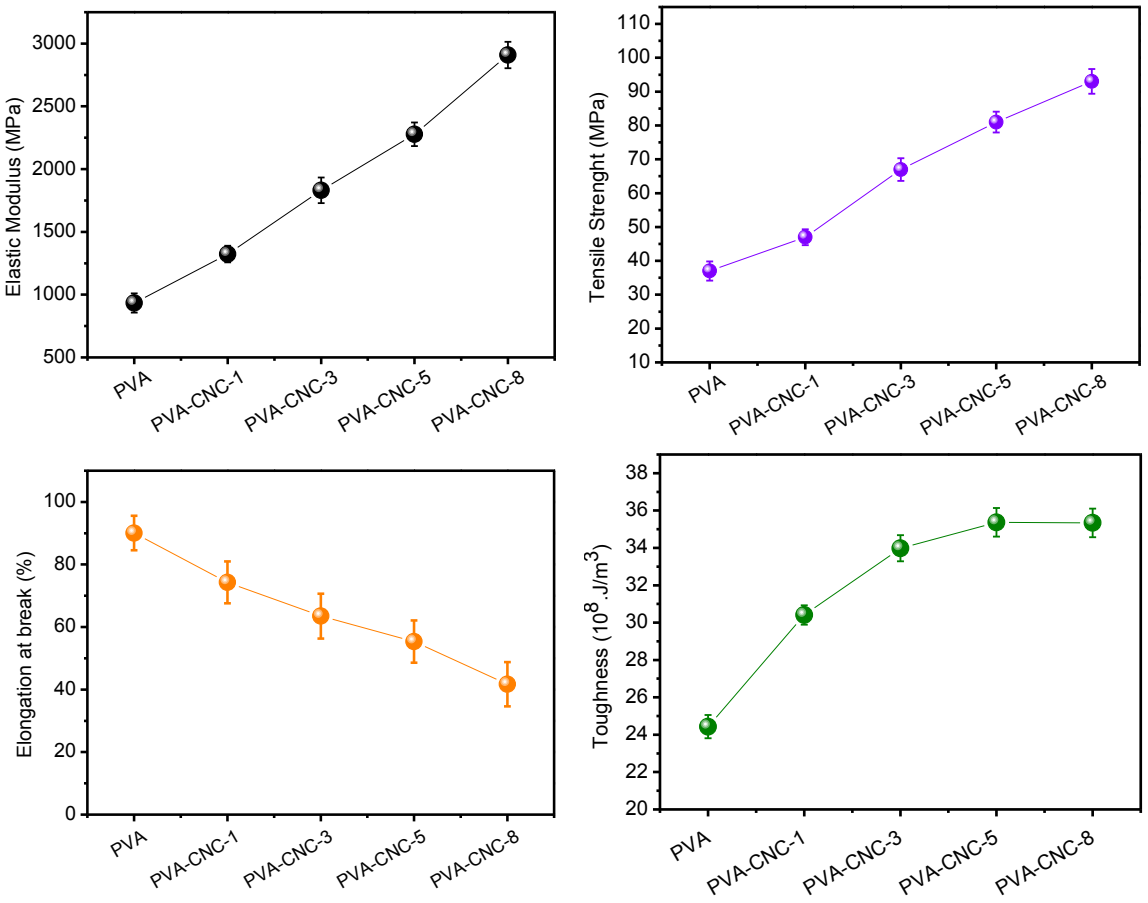


**Figure 11**: (a) Elastic modulus, (b) tensile strength and (c) elongation at break and (d) toughness of neat PVA and its nanocomposites.

**Table 1**: elemental analysis of AW, ATAW and BAW samples.

| Samples | C (%) | H (%) | O (%) | N (%) | S (%) |
|---|---|---|---|---|---|
| AW | 38.80 ± 0.02 | 5.63 ± 0.19 | 50.06 ± 0.02 | 4.82 ± 0.04 | 0.69 ± 0.01 |
| ATAW | 33.57 ± 0.19 | 4.56 ± 0.03 | 61.12 ± 0.07 | 0.35 ± 0.07 | 0.40 ± 0.04 |
| BAW | 37.47 ± 0.09 | 5.43 ± 0.32 | 56.87 ± 0.12 | 0.07 ± 0.07 | 0.13 ± 0.03 |

**Table 2**: Onset temperature ($T_{onset}$) and major maximum temperature ($T_m$) for all cellulosic samples

| Sample | $T_{onset}$ (°C) | $T_m$ (°C) |
|---|---|---|
| AW | 210 | 324 |
| ATAW | 212 | 334 |
| BAW | 234 | 349 |
| CNC30 | 201 | 331 |
| CNC40 | 185 | 278 |
| CNC80 | 134 | 215 |

**Table 3:** Moisture content (MC), onset temperature ($T_{onset}$), temperature corresponding to a weight loss of 10 % ($T_{10\%}$) and residual weight (RW) for neat PVA and PVA-CNC nanocomposite films.

| Samples | MC (%) | $T_{onset}$ (°C) | $T_{10\,\%}$ (°C) | RW (%) |
|---|---|---|---|---|
| **PVA** | 6.27 | 188.74 | 272.12 | 4.89 |
| **PVA-CNC-1** | 5.50 | 191.88 | 279.67 | 4.99 |
| **PVA-CNC-3** | 5.24 | 200.48 | 282.93 | 5.05 |
| **PVA-CNC-5** | 4.38 | 205.35 | 287.22 | 5.03 |
| **PVA-CNC-8** | 4.06 | 210.93 | 288.31 | 5.11 |

**Table 4**: Elastic modulus ($E$), Tensile strength ($\sigma$), Elongation at break ($\varepsilon$) and toughness ($T$) of neat PVA PVA-CNC nanocomposite films.

| Samples | $E$ (MPa) | σ (MPa) | ε (%) | $T$ ($10^8$.J/m3) |
|---|---|---|---|---|
| **PVA** | 933.79 ± 76.65 | 37.36 ± 2.85 | 90.07 ± 5.50 | 24.43 ± 0.62 |
| **PVA-CNC-1** | 1323.81 ± 66.15 | 47.47 ± 2.35 | 74.29 ± 6.71 | 30.41 ± 0.52 |
| **PVA-CNC-3** | 1761.60 ± 102.55 | 67.35 ± 3.45 | 63.50 ± 7.17 | 33.98 ± 0.69 |
| **PVA-CNC-5** | 2258.98 ± 93.90 | 81.67 ± 3.05 | 55.34 ± 6.17 | 35.37 ± 0.76 |
| **PVA-CNC-8** | 2939.35 ± 105.45 | 93.56 ± 3.65 | 41.72 ± 7.08 | 35.34 ± 0.77 |